

4D-Printed Biodegradable and Remotely Controllable Shape Memory Occlusion Devices

Cheng Lin, Jinxin Lv, Yuanshi Li, Fenghua Zhang, Jinrong Li, Yanju Liu, Liwu Liu,* and Jinsong Leng*

Implantation of occlusion devices is an effective approach for the treatment of congenital heart diseases in the clinic. However, most commercial clinical occlusion devices are currently made of nondegradable metals, which may lead to complications such as perforation, allergies, and erosion. In this work, 4D-printed novel, biodegradable, remotely controllable, and personalized shape memory occlusion devices are demonstrated and atrial septal defect occluders are exemplified. By incorporating Fe₃O₄ magnetic particles into the shape memory poly(lactic acid) matrix, the deployment of the occluders can be controlled remotely after implantation. The excellent cytocompatibility and histocompatibility are conducive to cell adhesion and ingrowth of granulation tissues into the occluders, thus facilitating rapid endothelialization. In addition, personalized shape memory occluders ensure an ideal fit and provide sufficient support for defects. Therefore, 4D-printed shape memory occluders can be used as a potential substitute for metal occlusion devices.

highly effective method for the treatment of CHDs.^[2,3] Most clinical occlusion devices, such as Amplatzer occluders (St. Jude Medical), Cera occluders (Lifotech Scientific), Occlutech Figulla occluders (Occlutech) and GORE HELEX occluders (W.L. Gore & Associates), are made of nitinol wires. These occluders can provide effective sealing but may still lead to severe complications, such as erosion, allergy and perforation.^[4] In this case, biodegradable occluders have emerged and are considered to be a promising alternative to metal occluders. Some biodegradable occluders have been developed, such as Biostar (partially absorbable), Chinese Lantern, and other types of absorbable occluders.^[4–8] However, the deployment processes of these occluders are uncontrollable. In addition, these occluders

1. Introduction

Congenital heart diseases (CHDs) are the most common congenital anomaly, occurring in 8 out of 1000 newborns.^[1] An atrial septal defect (ASD) is a CHD that allows abnormal blood flow from the left atrium to the right atrium. If left untreated, ASD may result in pulmonary hypertension and even heart failure. Interventional therapy is a percutaneous nonsurgical closure treatment that is increasingly accepted as a

generally have several certain specifications and cannot provide personalized devices for patients.^[9,10]

Fortunately, the emergence of 3D printing technology has created new opportunities for fabricating personalized medical devices in a rapid, cost-effective manner.^[11] The personalized devices can significantly improve the accuracy of treatment.^[12–14] Therefore, 3D printing has broad application prospects in tissue engineering.^[15–17] Shape memory polymers (SMPs), a class of intelligent materials, are able to respond to external stimuli, such as heat, light, solutions, electrical fields and magnetic fields.^[18] Recently, SMPs have shown great potential in the biomedical field, such as drug-release devices,^[19] various scaffolds,^[20–22] self-tightening sutures,^[23] embolization,^[24–26] and orthopedic devices.^[27–29] Furthermore, the application of shape memory polymers in a minimally invasive treatment provides a highly controllable and customized deployment in vivo.^[30] Hu and co-workers proposed a shape memory PU/HA bone repair foam with an excellent self-fitting capacity and verified that the foam was capable of perfectly matching the defect by implantation in vivo.^[31] Hence, with the introduction of intelligent material (such as SMPs), 3D-printed architectures are capable of changing their shapes, properties, or functionalities over time. This introduces a new term, namely, 4D printing, which adds a fourth dimension (time) to 3D printing. After first being reported in 2013, 4D printing has generated tremendous research interests.^[32,33] Cohn et al. presented a 4D-printed shape memory tracheal stent. After implantation, the stent can recover from the contracted shape to its original shape under the

C. Lin, Prof. Y. Liu, Prof. L. Liu
Department of Astronautical Science and Mechanics
Harbin Institute of Technology (HIT)
P.O. Box 301, No. 92 West Dazhi Street
Harbin 150001, P. R. China
E-mail: liulw@hit.edu.cn

J. Lv, Dr. Y. Li
Department of Cardiology
First Affiliated Hospital of Harbin Medical University
23 Youzheng Street, Nangang District, Harbin
Heilongjiang 150001, P. R. China

Dr. F. Zhang, J. Li, Prof. J. Leng
National Key Laboratory of Science and Technology On Advanced Composites in Special Environments
Harbin Institute of Technology (HIT)
No.2 Yikuang Street, P.O. Box 3011
Harbin 150080, P. R. China
E-mail: lengjs@hit.edu.cn

DOI: 10.1002/adfm.201906569

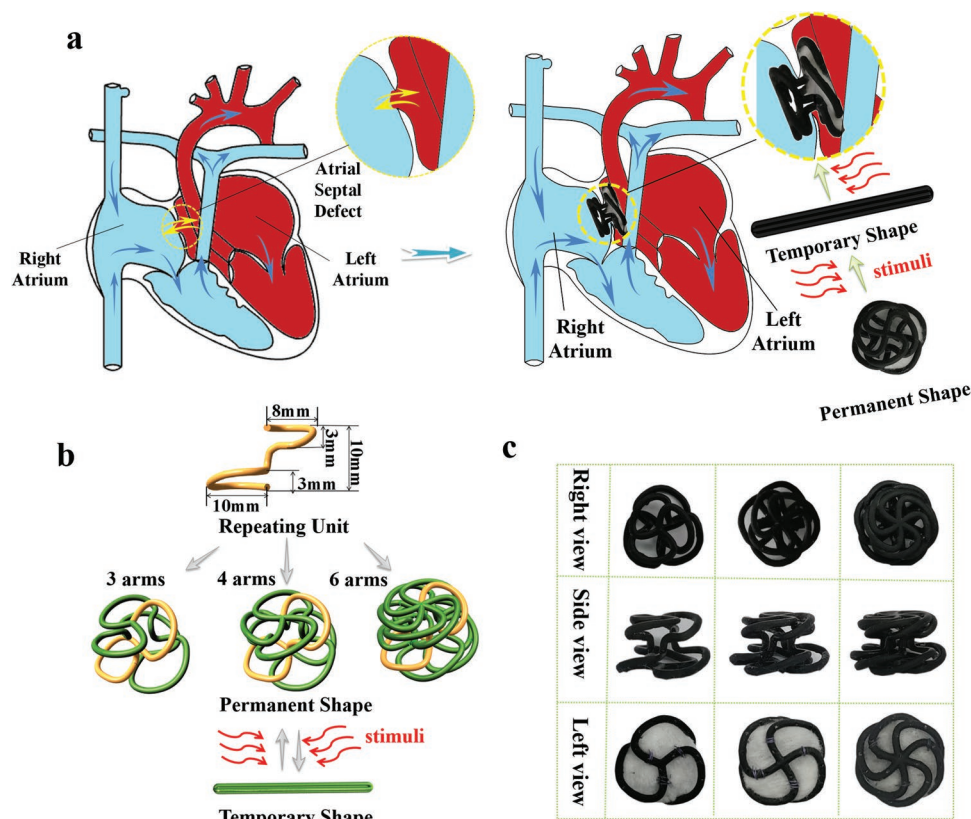


Figure 1. a) Schematic illustration of the ASD prototype before and after interventional therapy with an occluder; b) schematic illustration of the design of three types of occluder frames with different arms; c) 4D-printed occluders with frame and membranes

stimulus of a local increment in temperature. In addition, the personalized stent ensured accurate positioning and stable fixation.^[21] Despite many reports of 3D- or 4D-printed stents,^[34–39] few studies have used this technique for congenital heart defects.

Here, 4D-printed shape memory occluders were developed to facilitate a temporary platform for ASD before tissue endothelialization. **Figure 1a** illustrates an ASD prototype before and after interventional therapy with an occluder. The occluder consists of a supporting frame and thin occluding membranes covering the frame. The frame was fabricated by 4D printing technology, and shape memory poly(lactic acid) (PLA)-based magnetic nanocomposites were used to print three types of occluder frames with different numbers of arms (3/4/6 arms). Fe_3O_4 nanoparticles are highly biocompatible biomedical functional materials.^[40] By incorporating Fe_3O_4 magnetic particles into the PLA matrix, the composites can respond to the magnetic field. This magnetic driven approach is regarded to be a safe and controllable method^[41–44] and is especially suitable for noncontacted actuation in enclosed and restricted spaces.^[45] The occluding membranes were prepared by an electrospinning technology that uses shape memory PLA. Because of its similarity with the tissue extracellular matrix, the prepared fibrous porous membrane can be used as a substrate to guide cell adhesion, growth and proliferation.^[46] Hence, the membranes can be more effective and can shorten the endothelialization time.^[47] The unique structural design of the occluder, combined with shape memory

performance, ensured large deformation from a permanent shape to a temporary shape and would facilitate interventional therapy. Then, the mechanical properties, cytocompatibility, histocompatibility, shape memory properties under a magnetic field and the in vitro feasibility of occluders were systematically investigated.

2. Results and Discussion

The design diagram of the occluder frame is illustrated in Figure 1b. The occluder frame is double disc-shaped with a thin waist in the middle. According to the number of repetitive units, the frames are divided into 3 arms, 4 arms, and 6 arms. The process of implantation and deployment of the 4D-printed shape memory occluder is described as follows (Figure 1a,b): first, the occluder is programmed from a permanent double disc shape into a temporary linear shape under a stimulus (e.g., heat and magnetic field), and the linear temporary shape is used to reduce the size of the scar in interventional surgery. Second, the occluder recovers to its permanent shape under a stimulus after implantation. Figure 1c shows the printed occluders with membranes. Figure S1 (Supporting Information) shows the scanning electron microscope (SEM) images of shape memory PLA occluder membranes. The membranes were sutured to the left disc of the occluder frame to prevent blood flow, promote cell adhesion and shorten the time of endothelialization. Since

the promotion of fibrous porous membranes on cell growth has been comprehensively investigated previously,^[46–48] it will not be revisited here.

2.1. Mechanical Properties of Shape Memory Occluders

Mechanical properties are critical for tissue engineering implants, since they will be subjected to complex physiological loads after implantation. To study the mechanical properties of the Fe₃O₄–PLA composites and their evolution after implantation, uniaxial tensile tests were conducted using 3D printed dumbbell shaped samples. **Figure 2a** displays the stress–strain curves of the samples at body temperature (37 °C). For convenience, Fe₃O₄–PLA is abbreviated as mPLA. As shown in Figure 2a, the strength of 5 wt% mPLA, ≈60 MPa, was highest among the five materials, and was much higher than that of the pure shape memory PLA. The strength of 10 wt% mPLA was slightly lower than that of 5 wt% mPLA, which was ≈58 MPa.

The strengths of the 5 wt% mPLA, 10 wt% mPLA and 15 wt% mPLA composites were higher than that of pure PLA, which indicated that rigid particles played an important role in reinforcing the polymer matrix. The increase in the tensile strengths of the composites was due to the transfer of stress from the polymer matrix to rigid particles.^[49] The strengths and elongation of the 20 wt% mPLA composites decreased slightly because of the existence of large clusters of Fe₃O₄ nanoparticles. Nevertheless, the strengths of all the composites were significantly higher than those in the literature (≈14 MPa).^[50] In addition, Young's modulus of the mPLA composites increased markedly with the increase of the Fe₃O₄ concentration. Massive crazing is one of the toughening mechanisms of polymers.^[49] Compared with the pure PLA, 10 wt% mPLA exhibited an obvious toughening behavior and yielded a short quasi-constant stress regime. This phenomenon might be due to the detachment between the rigid Fe₃O₄ particles and the polymer matrix during loading, and there were more opportunities for the microvoids to develop into massive crazing. This result was

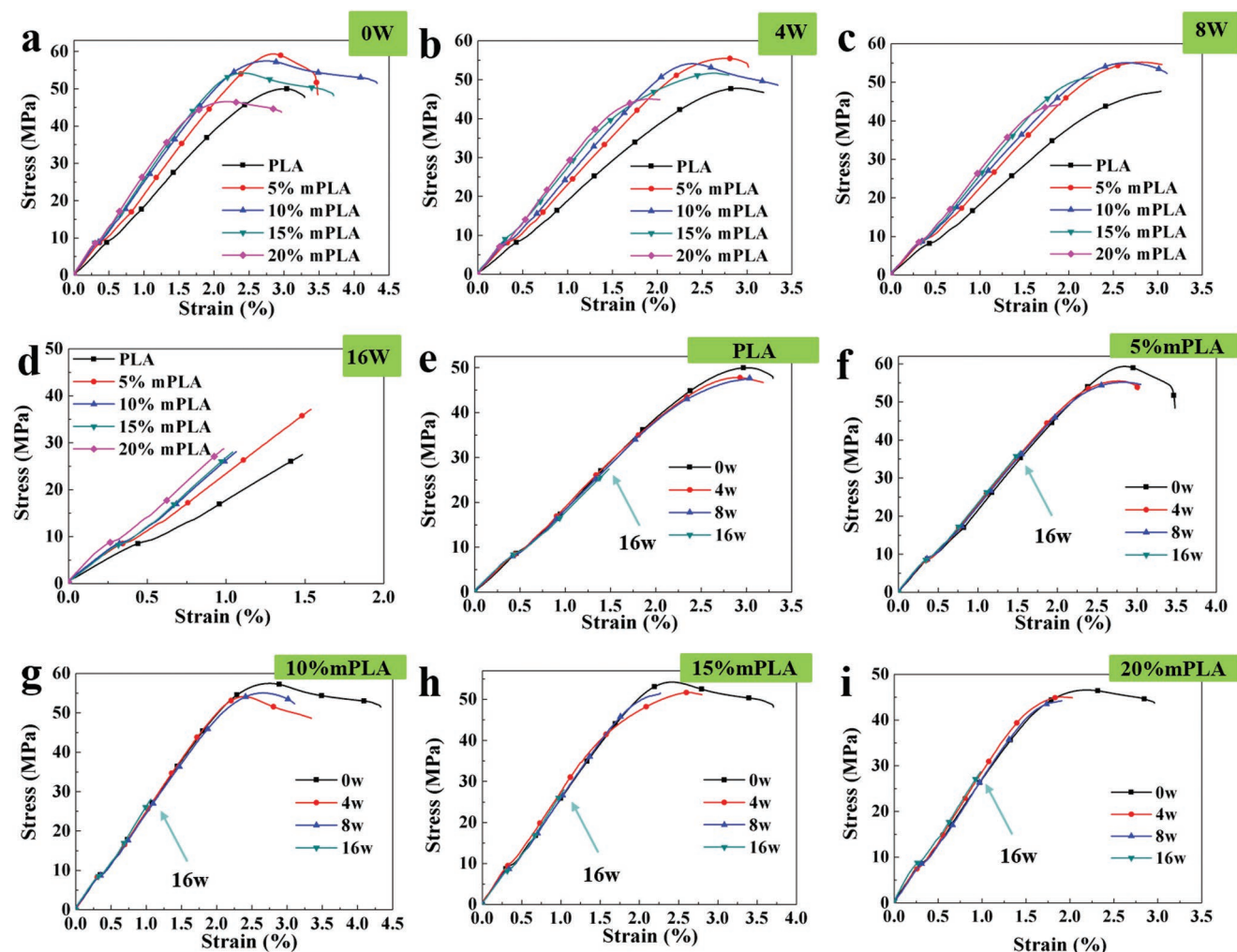


Figure 2. Uniaxial tensile stress–strain curves (37 °C) of the shape memory PLA and mPLA composites with different concentrations of Fe₃O₄ particles degraded for a) 0 weeks, b) 4 weeks, c) 8 weeks, and d) 16 weeks; uniaxial tensile stress–strain curves (37 °C) at different degradation times: e) PLA; f) 5 wt% mPLA, g) 10 wt% mPLA, h) 15 wt% mPLA, and i) 20 wt% mPLA. The arrows in the e–i) point to the end points of the stress–strain curves of the specimens were degraded for 16 weeks. For convenience, Fe₃O₄–PLA is abbreviated as mPLA.

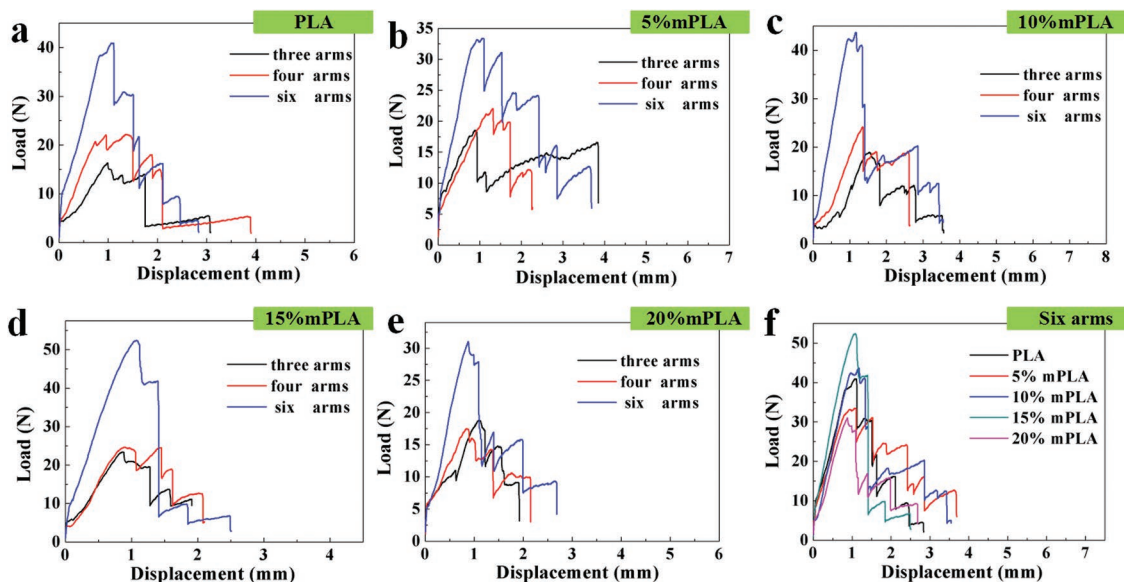


Figure 3. Load–displacement curves (37 °C) of shape memory occluders: a) PLA, b) 5 wt% mPLA, c) 10 wt% mPLA, d) 15 wt% mPLA, and e) 20 wt% mPLA; f) 6-arm occluders with different Fe₃O₄ concentrations. For convenience, Fe₃O₄–PLA is abbreviated as mPLA.

verified by the SEM fracture surfaces of PLA and 10 wt% mPLA samples, as displayed in Figure S2 in the Supporting Information. It was evident that there was more crazing in the 10 wt% mPLA fracture surface than in PLA.^[49]

The effect of degradation *in vitro* on the mechanical properties of mPLA composites was characterized to evaluate the change of mechanical properties of mPLA composites with time after implantation. The samples immersed in phosphate buffered saline (PBS) solution were taken out and subjected to uniaxial tensile tests at predetermined time points. Figure 2 shows the uniaxial tensile stress–strain curves of mPLA composites at different degradation times. After 4 and 8 weeks of degradation, the strengths of the samples were almost unaffected, but the %elongations at the break decreased slightly. After 16 weeks of degradation, the strength decreased by 50–60%, and the samples were fractured in a brittle manner. This phenomenon might be due to the breakage of polymer chains caused by hydrolysis, resulting in the formation of substances with low molecular weight, such as oligomers and monomers. The stability of polymer chains was destroyed, so the strength and %elongation at the break of the polymer were reduced. Nevertheless, it is worth noting that even after 16 weeks of degradation, the strength remained at 30 MPa, which was more than twice the 14 MPa that was reported in the literature.^[50] The Young's modulus, strengths, and %elongation at break of the shape memory PLA and mPLA composites at different degradation times are shown in Figures S3–S5 (Supporting Information). In addition, the weight of the specimens decreased slightly after 16 weeks of degradation. The weight of 5 wt% mPLA, 10 wt% mPLA, 15 wt% mPLA and 20 wt% mPLA decreased by 0.22%, 0.20%, 0.26%, and 0.15%, respectively.

Because of the complexity of the physiological load, it is necessary to determine whether the occluder can provide adequate support after implantation. The waist of the occluder is vital for load carrying and the load carrying capacity of the waist was examined using the customized clamp illustrated in Figure S6

(Supporting Information). **Figure 3** shows the uniaxial tensile load–displacement curves of the shape memory occluders. The stepped curve was related to the structure of the occluders. When the tension reached the ultimate load carrying capacity of the occluder, the arms broke in turn. As shown in Figure 3a–e, the 6-arm occluders had the highest load carrying capacity, while the 4-arm and 3-arm occluders had lower load carrying capacities. For 4-arm occluders, the load carrying capacities of 10 wt% mPLA and 15 wt% mPLA were ≈25 N. Figure 3f shows the load–displacement curves of 6-arm occluders with different Fe₃O₄ concentrations. It can be seen that 15 wt% mPLA had the highest load carrying capacity, followed by 10 wt% mPLA. The waist of 20 wt% mPLA occluders had the lowest load carrying capacity due to the existence of large clusters of nanoparticles. In addition, the load carrying capacity of the occluder waist was compared with the pressure between the left and right atria to assess whether the occluder can withstand atrial pressure (Table S1, Supporting Information).

To evaluate the ability of the occluder to resist the compression load after implantation, compression tests were conducted and the results are shown in **Figure 4**. The maximum load of the compression test was set at 50 N, which was much greater than the force of the left and right atrial pressure difference on the occluder disc. As shown in Figure 4a–e, the occluders of mPLA with different Fe₃O₄ concentrations showed similar compression behaviors. The load–displacement curves were generally divided into two sections. The first section was the “elasticity zone”; the second section was the “densification zone,” and the slope of the second section greatly increased.^[51] Under the same compression load, the displacement of the 6-arm occluder was the smallest, indicating that the stiffness was the largest, while the displacement of the 4-arm occluder was the largest, indicating that the flexibility was the best. The 3-arm occluders showed a small number of sawtooth on the curve due to fewer arms and poor stability. Interestingly, due to the unique structures, the occluders remained intact

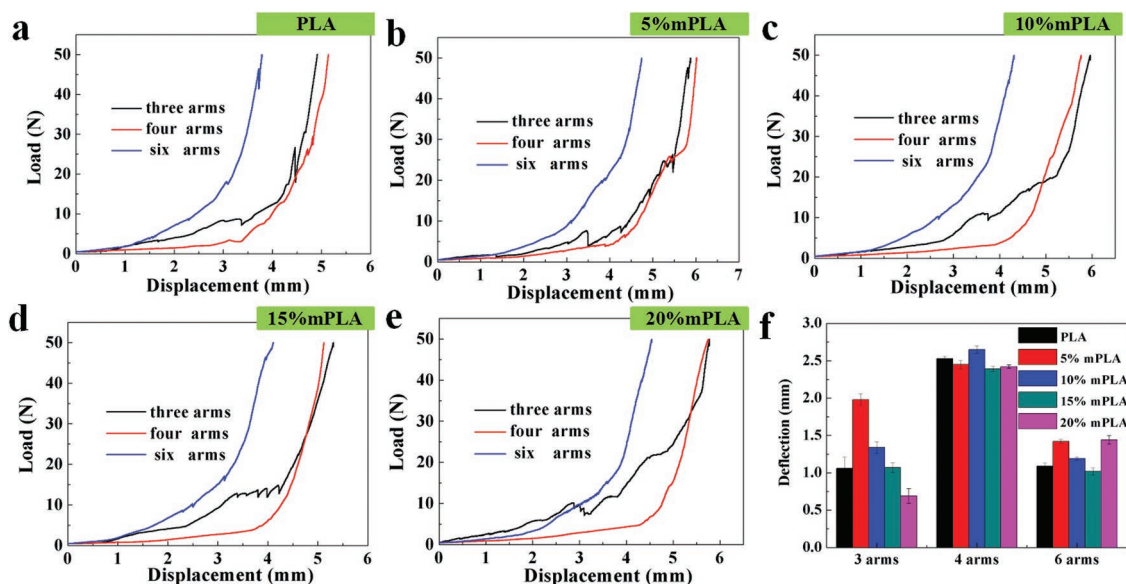


Figure 4. Compressive behavior of occluders: a) PLA, b) 5 wt% mPLA, c) 10 wt% mPLA, d) 15 wt% mPLA, and e) 20 wt% mPLA occluders with different arms; f) deflections of occluders with different Fe_3O_4 concentrations under 2 N compression load. For convenience, Fe_3O_4 -PLA is abbreviated as mPLA.

after being subjected to a 50 N compression load and had high resilience rates (Figure S7, Supporting Information). Compared with the compression test results of the PCL occluder and the Amplatzer occluder (St. Jude Medical, Minneapolis, MN) in the literature,^[4] the range of deflections of our 4D-printed shape memory occluders was 0.8–2.7 mm (Figure 4f), which was smaller than those of the PCL occluder (≈ 7 mm) and the Amplatzer occluder (≈ 9 mm) under the same compression load (2 N). This result showed that the 4D-printed shape memory occluder was more stable than the Amplatzer occluder and PCL occluder.^[4]

2.2. Cytocompatibility of Shape Memory Occluder Materials

After implantation, the occluder will serve as a temporary platform for cell growth and adhesion to complete the closure of the defect; the process is known as endothelialization. Therefore, it is critical to evaluate the cytocompatibility of the materials, and an *in vitro* cardiomyocytes culture was conducted. Figure 5 shows the merged fluorescent images of the cardiomyocytes that were cultured in different plates for 1, 3, and 5 days. The living cells were stained green, and the dead cells were stained red. After 1 day of culture, some cells adhered and proliferated on the surface of the culture plates. The surfaces of the 15 wt% mPLA (Figure 5d) and 20 wt% mPLA (Figure 5e) plates showed relatively sparse cell distribution. After 3 days of culture, the proliferation of cells increased significantly, and the number of cells on the surface of the 5 wt% mPLA plate was significantly higher than that of PLA. After 5 days of culture, due to the significant increase in cell density, several dead cells were observed on the surfaces of the plates. The cells cultured in mPLA groups proliferated more than those cultured in the PLA groups. Therefore, the addition of Fe_3O_4 particles can increase cell adhesion and proliferation. This phenomenon might be due to the increased surface roughness and hardness

of the mPLA composite plates resulting in mechanical feedback and activation of the stress-sensitive ion channels, thereby increasing cell adhesion stability and contraction strength to promote cell growth.^[52] The effective proliferation of cells indicated the excellent cytocompatibility of mPLA composites, which is beneficial to endothelialization after implantation.

2.3. Histocompatibility of Shape Memory Occluders

The occluders were subcutaneously implanted into Sprague-Dawley (SD) male rats and the histocompatibility of the occluders were assessed based on tissue response. The adjacent tissues of the occluders were collected to monitor the histological changes after implantation by standard hematoxylin-eosin (H&E) staining. The implantation process is shown in Figure 6a. The gross inspection of occluders and the H&E-stained adjacent tissues of occluders at different weeks after implantation are respectively demonstrated in Figure 6b,c. Once implanted, the foreign body reaction will be initiated, which is the self-protected form of the host. The reaction consists of acute phase responses and chronic phase responses.^[53] When entering the host, the implant is quickly covered by a nonspecific protein layer, and inflammatory cells extravasate from blood vessels to the implant. In parallel, cytokines and angiogenic factors will be secreted to intensify inflammation and induce angiogenesis, respectively. This acute phase response is usually the strongest after 1 week of implantation, then gradually subsides.^[54] As shown in Figure 6c, in the first week after implantation, the histologic examination showed massive inflammatory cell infiltration (denoted by black arrowheads, Figure 6c) and newly formed microvessels (denoted by blue circles, Figure 6c). The gap between the arms of occluder was filled with tissues. The left disc was covered with tissues, while there was almost no tissue wrapping on the surface of the right disc (the disc without occluding fibrous membranes). This

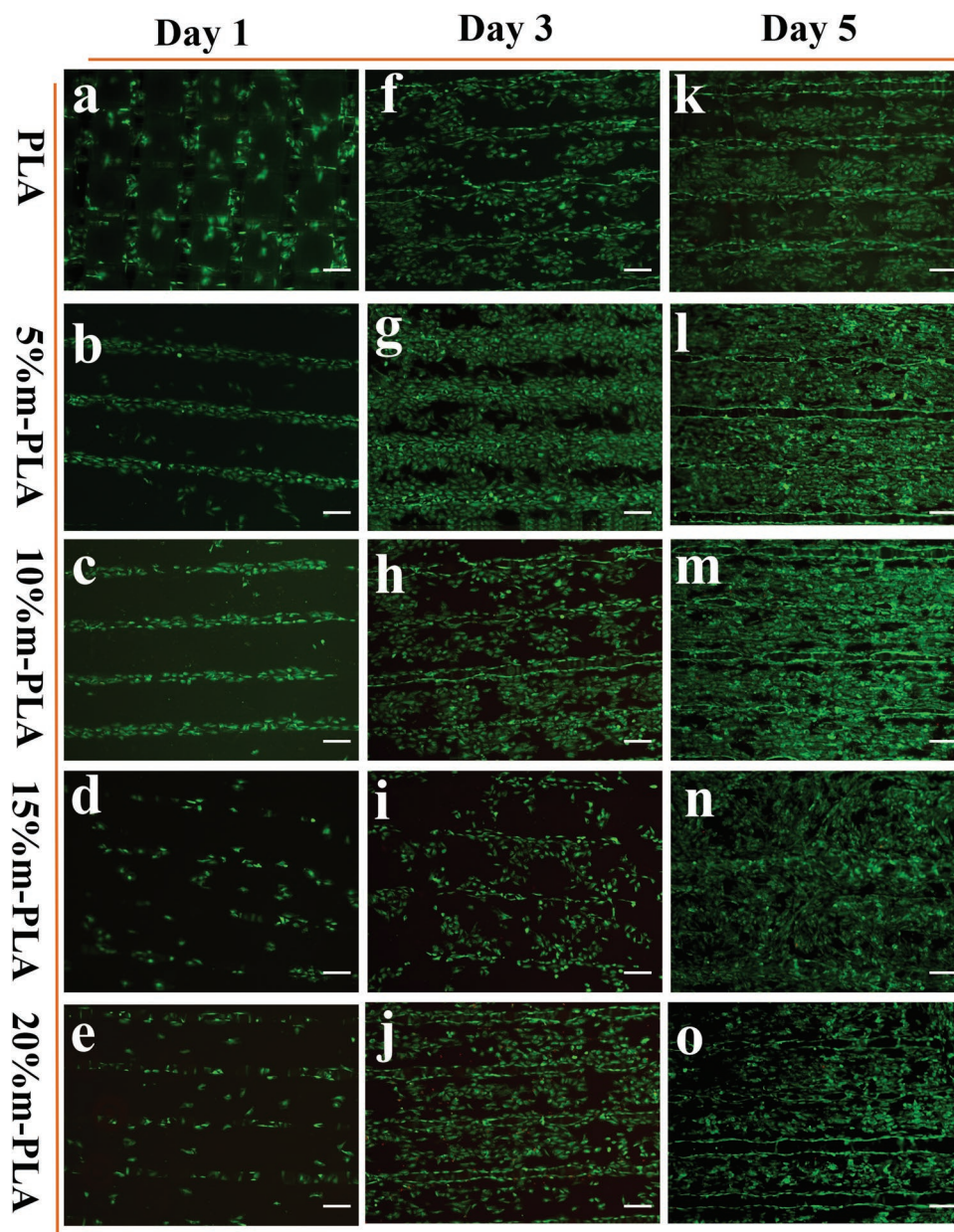


Figure 5. Merged fluorescent images of the cardiomyocyte cells cultured in shape memory PLA and mPLA composites with different concentrations of Fe_3O_4 for 1, 3, and 5 days. The living cells were stained green, and the dead cells were stained with red. Scale bar: 200 μm

phenomenon confirmed that occluding fibrous membranes can promote endothelialization.

Chronic phase responses follow acute phase responses. At this stage, fibroblasts proliferate and the implant will be wrapped in a fibrous capsule.^[54] At 2 weeks, the number of inflammatory cells decreased significantly, and fibroblasts (denoted by red arrowheads, Figure 6c) were observed. Fibrous granulation tissues grew into the occluder, and the surface of the right disc was covered with tissues. Meanwhile, due to the multi-stage hydrolysis, the material was gradually fragmented and granulated.^[55,56] Large degraded particles could be observed (denoted by yellow arrowheads, Figure 6c), which confirmed the degradability of the material. At 4 weeks, the

large degraded particles continued to degrade into small particles (Figure 6c) and the presence of the occluding membranes cannot be accurately distinguished (Figure 6b). The occluding membranes were completely covered by a continuous neo-endothelium and a thin layer of poorly vascularized young granulation tissues.^[57] After 6 weeks, more degraded particles of occluding membranes could be found (Figure 6c). A large number of leached blood cells, longitudinally cut blood vessels (blue arrowheads), and degraded particles were distributed in the connective tissues at 8 weeks. The corresponding images (Figure 6b) also showed a bright red color. The blood cells might have appeared due to the increase in neovascularization, and they were ruptured during the explanation of the

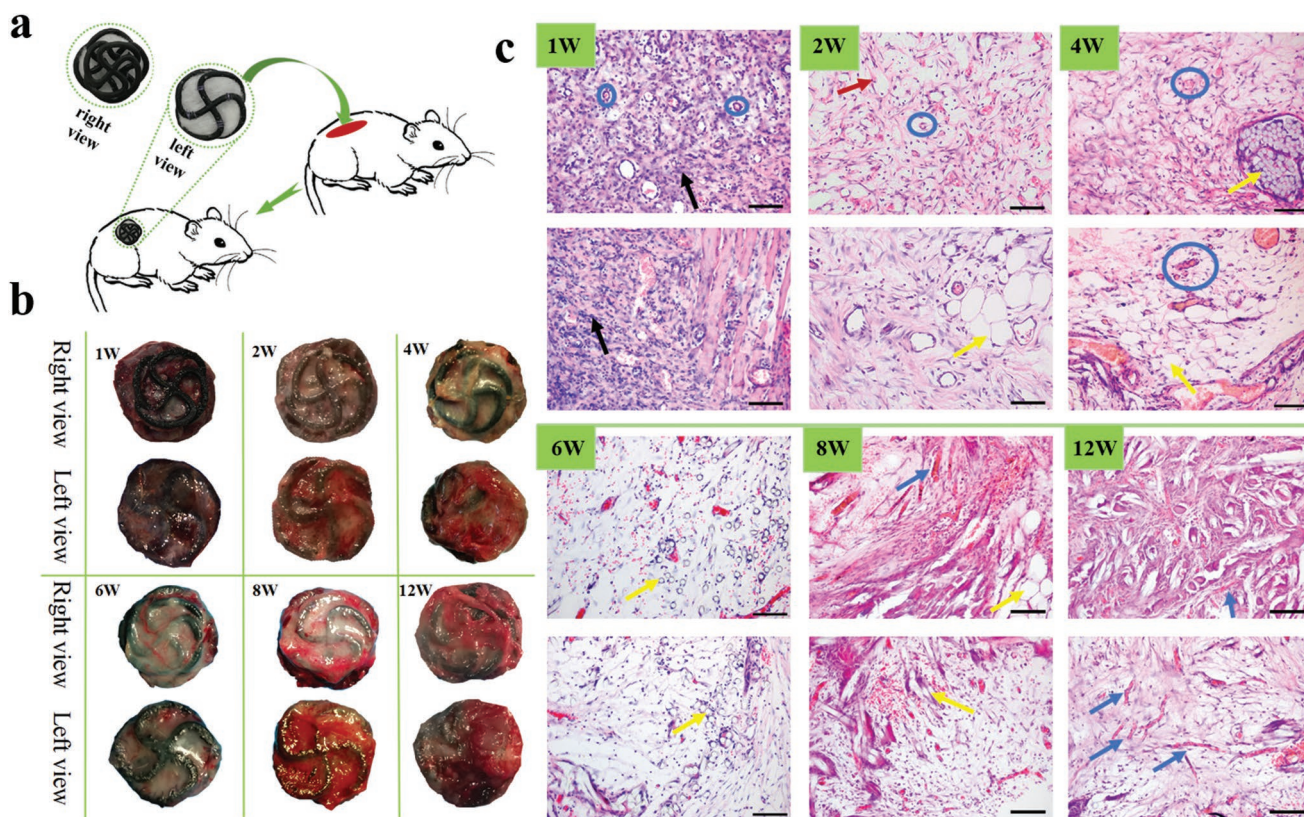


Figure 6. a) Schematic illustration of the implantation process; b) gross inspection of occluders; c) H&E-stained adjacent tissues of occluders at different time points after implantation, scale bar: 400 μm . Original magnification: 200 \times . Inflammatory cells: black arrowheads; fibroblast: red arrowheads; newly formed microvessels: blue circles; degraded particles: yellow arrowheads; blood vessels: blue arrowheads.

occluder. By 12 weeks, a large amount of longitudinally cut blood vessels (blue arrowheads) were distributed in the connective tissue.

In conclusion, occluder implantation caused a foreign body reaction; newly formed microvessels can be observed after 1 week; and the degraded particles can be seen after 2 weeks. The results demonstrated good histocompatibility and degradability of the occluders.

2.4. Shape Memory Properties and Controllable Deployment of Shape Memory Occluders

The shape memory process of the thermally induced SMPs can be described as follows: When the SMPs in the permanent shape (i.e., the original shape) are heated to $T > T_{\text{trans}}$ (a transition temperature, T_{trans}), which is equal to a melting temperature (T_m) or a glass transition temperature (T_g), the SMPs become soft. For the shape memory PLA and mPLA, $T_{\text{trans}} = T_g$, the values are $\approx 65\text{--}67^\circ\text{C}$ (Figure S8, Supporting Information). Then, the SMPs can be programmed into a temporary shape under the external force, and the temporary shape is fixed upon $T < T_{\text{trans}}$. When reheated to $T > T_{\text{trans}}$, the SMPs recover to permanent shape automatically. For magnetic-induced SMPs, the incorporated magnetic particles act as inductive heaters in alternating magnetic fields to heat the SMPs, which possess the advantage of remote and selective actuation.

The magnetically induced shape memory behaviors of mPLA composites with different Fe_3O_4 concentrations were investigated under an alternating magnetic field with a frequency of 27.5 kHz and a field strength of 4 kA m^{-1} . The results showed that 5 wt% mPLA cannot be actuated due to the low concentration of magnetic particles (fewer induction heaters). When the concentration of magnetic particles increased to 10 wt%, the samples can respond to the magnetic field. The shape recovery ratios (R_f) of 10 wt% mPLA, 15 wt% mPLA, and 20 wt% mPLA were 94.27%, 95.58%, and 94.58%, respectively, which demonstrated their excellent shape recovery properties. The recovery processes and calculation details of R_f are shown in the Supporting Information (Figures S9 and S10, Supporting Information).

Considering the mechanical properties, shape memory properties, and biocompatibility of the four kinds of mPLA with different Fe_3O_4 concentrations, 10 wt% mPLA possesses the best comprehensive properties. In addition, the larger size of the delivery catheter is needed for the occluder with more arms. To reduce the catheter size and to account for the mechanical properties of the occluder, the 10 wt% mPLA 4-arm occluder was considered to be the optimal type of occluder. Figure 7a exhibits the shape recovery process of the 10 wt% mPLA 4-arm occluder under a magnetic field. Only 22 s were required for the 10 wt% mPLA occluder to recover to its original shape. The magnetic field response time was ≈ 10 s, and the recovery process was completed in the next 12 s. The recovery ratio (R_f)

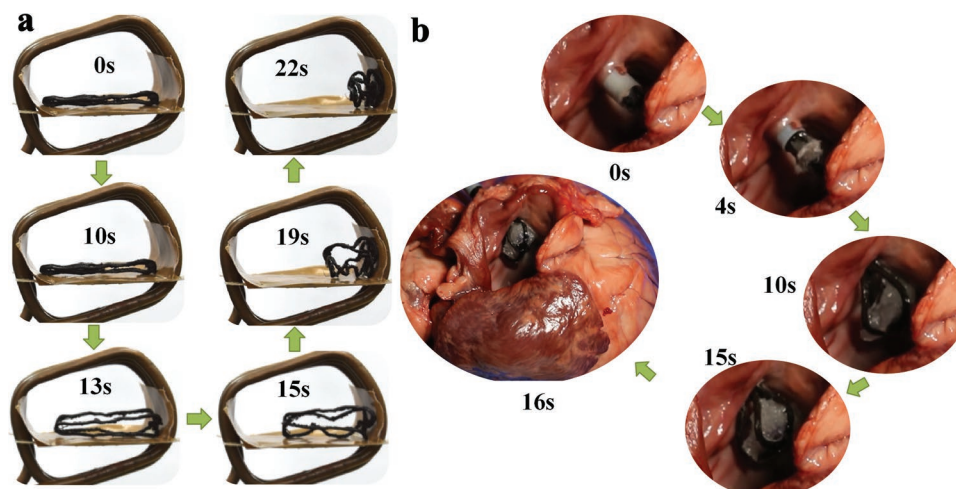


Figure 7. a) Programmed shape recovery process of a 10 wt% mPLA 4-arm occluder under a magnetic field and b) an in vitro feasibility study of an ASD occluder

was $\approx 95\%$ (the calculation method is shown in Figure S10 in the Supporting Information). After five deformation cycles, the recovery ratio of the occluder remained above 90% (Figure S11, Supporting Information).

2.5. Feasibility Study of Shape Memory Occluders In Vitro

The in vitro feasibility study of six occluders was conducted to investigate the ease of occluder deployment, and a 14 Fr. catheter (Starway Medical Technology Inc.) was used to load the occluder. As shown in Figure 7b, the occluder can be packaged, delivered and released smoothly through the catheter, and the deployment process of the occluder was completed within 16 s. All the occluders were properly deployed. After occlusion, the heart was dissected. The ASD was located in the middle of the foramen ovale, and the distance between the ASD and the mitral/tricuspid/coronary sinus/right superior pulmonary vein was more than 2 mm, which indicated that the location of the ASD was suitable for occlusion. More importantly, all the occluders completely closed the defect without displacement.

3. Conclusion

In summary, 4D-printed biodegradable, remotely controllable, personalized shape memory occluders were developed. Although the current study still has some limitations. The glass transition temperature of the occluder needs to be lowered, such as modifying PLA with biocompatible plasticizers.^[22,58–60] The 4D-printed shape memory occluder deserves further study, as it successfully addresses some of the key drawbacks marring nondegradable metal occlusion devices. First, the occluder can promote cell adhesion, proliferation and tissue growth, facilitating the rapid endothelialization. However, metal occluders may even cause allergies and erosion. Second, the occluder is biodegradable, avoiding the potential danger of metal occluder remaining in the body forever.

Other advantages of the 4D printed shape memory occluder are summarized as follows. Personalized occluder can be programmed to linear temporary shape and the deployment process is remotely controllable, thus reducing the scar size during intervention and improving the success rate of clinical occlusion. The occluder can provide sufficient mechanical support for sealing defects even after 16 weeks of degradation in vitro and seal the defects completely and rapidly. It is worth mentioning that the ASD occluder is used as an example in this study, other types of occluders (e.g., ventricular septal defect occluders and left atrial appendage occluders) can also be designed and fabricated in a similar way. Therefore, it is expected that the 4D-printed shape memory occluder can become a promising occlusion device and this study pave the way for its further development.

4. Experimental Section

Preparation of PLA and Fe_3O_4 -PLA Composite Filaments: First, the PLA pellets (Nature Works LLC. Ingeo 4032D) and the Fe_3O_4 nanoparticles (Shanghai Macklin Biochemical Co. Ltd., 99.5%, 20 nm) were melt-blended, and the homogeneous mixture was extruded through a corotating twin-screw extruder (CTE20 PLUS, Coperion Nanjing Machinery Co., Ltd). The mass fractions of Fe_3O_4 particles in the mixtures were 5, 10, 15, and 20 wt%. Then, the composite filaments were extruded from a nozzle with a diameter of 1.75 mm at extrusion temperature of 200 °C. The fabrication process of pure PLA filaments is similar to that of Fe_3O_4 -PLA filaments, except that no Fe_3O_4 magnetic particles were added to the PLA matrix.

Fabrication of Occluder Frames: The models of the occluders were constructed on the Siemens PLM Software UG NX 9.0. The diameter of the left disc, the diameter of the right disc, the height of the thin waist and the total height of the occluder were 20, 16, 4, and 10 mm, respectively. The size of the occluder was determined according to reference.^[3] In addition, the linewidth of the occluders was 1.1 mm. The constructed models were then exported as printable STL files and were printed by a fused deposition modeling (FDM) 3D printer (Anycubic i3 Mega, Shenzhen, China). The nozzle diameter, printing temperature and printing speed were 0.4 mm, 200 °C and 5 mm min⁻¹, respectively. Absorbable PGA surgical sutures (Shanghai Pudong Jinhuan Medical Products Co., Ltd.) were used to sew the fabric to the left disc.

Preparation of Occluder Membranes: The PLA particles were dispersed in dichloromethane at a concentration of 8 wt%, and electrospinning was carried out at room temperature (25 °C) after magnetic stirring for 24 h. The distance between the needle of syringe and the aluminum collecting mat was 175 mm. The applied voltage and flow rate were 15 kV and 1.5 mL h⁻¹, respectively. The average thickness of each membrane was ≈0.05 mm and each occluder contained three membranes. The morphologies of membranes were studied by VEGA3 TESCAN scanning electron microscope and the accelerating voltage was 20.0 kV.

Mechanical Property Tests: Uniaxial tensile tests were performed according to ASTM D638 to evaluate the stress–strain behaviors of the shape memory mPLA with different Fe₃O₄ concentrations (5, 10, 15, and 20 wt%). The dumbbell shaped samples were printed with dimensions of 115 mm × 6 mm × 2 mm. The samples were clamped at a certain distance between the grips. The samples were subjected to tension until failure with a preload of 1 N. The fracture surface morphologies of the samples were also examined by SEM at an accelerating voltage of 20.0 kV.

The load carrying capacities of the occluder waists were investigated using a customized clamp. As shown in Figure S3 (Supporting Information), the center of the clamp has a small hole with a diameter of 8 mm, which was approximately half the size of the occluder discs and slightly larger than the size of the occluder waist. The occluder was placed at the center of the clamp, and the uniaxial tension test was carried out. The hole in the clamp was used to simulate an atrial septal defect. The preload was 0.5 N and the uniaxial compression tests of occluders were performed between the two plate clamps until the maximum load was 50 N.

All mechanical tests were conducted on a Zwick 010 (Zwick GmbH & Co. KG, Germany) at the temperature of 37 °C with a loading speed of 2 mm min⁻¹. In each case, five samples were tested to obtain an average value. The samples were heated from 25 to 37 °C at a heating rate of 5 °C min⁻¹, then were maintained for another 15 min before testing.

In Vitro Degradation: The printed dumbbell shaped samples were immersed into a PBS solution (pH 7.2–7.4) in an incubator at 37 °C, and the solution was replaced weekly. The samples were removed at the preset time points for weight measurement and mechanical testing.

The degraded samples were rinsed in distilled water and then dried under vacuum at 37 °C until constant weight. The percentage of weight loss was calculated by

$$\text{weight loss (\%)} = \frac{m(t) - m_0}{m_0} \times 100\% \quad (1)$$

where m_t is the weight of the specimen on week t after degradation and m_0 is the original weight before degradation.

Shape Memory Behaviors: The shape memory behavior of Fe₃O₄–PLA bar samples with different Fe₃O₄ concentrations was characterized. The samples were printed with dimensions of 60 mm × 10 mm × 2 mm. The samples were then heated above T_{trans} (67 °C) in an oven and were bent into a U shape. After cooling, the temporary shape was fixed, and the samples were actuated under an alternating magnetic field with a frequency of 27.5 kHz and a field strength of 4 kA m⁻¹. Similarly, the occluder was deformed to a linear temporary shape when $T > T_{\text{trans}}$, and then the occluder was driven under the same alternating magnetic field. The shape recovery processes were recorded.

Cell Culture: To evaluate the proliferation of cardiomyocytes on different composition ratios of mPLA, round plates were printed with a diameter of 15 mm and a thickness of 1 mm. The plates were sequentially sterilized with absolute ethanol for 12 h, 75% absolute ethanol for 12 h, washed with PBS three times, and then exposed to ultraviolet light for 12 h. After sterilization, the printed plates were immersed in the culture medium of an RPMI-1640 medium supplemented with 10% fetal bovine serum and 1% penicillin/streptomycin for 12 h and then were gently placed at the bottom of each culture well. The cardiomyocytes were seeded onto the sterilized printed plates in each well at a density of 5×10^5 cells cm⁻². The cells and plates were cocultured for another 1, 3, and 5 days in a humidified incubator with 5% CO₂ at 37 °C. For

each group, six plates were used in parallel. The proliferation of cardiomyocytes was examined using LIVE/DEAD staining (Calcein-AM/PI, Dojindo).

In Vivo Histocompatibility Analysis: The study was approved by the Ethics Committee of the First Affiliated Hospital of Harbin Medical University. Considering the number of animals, the 10 wt% mPLA occluders were selected to evaluate the histocompatibility in vivo. Eighteen Sprague–Dawley male rats weighing about 350 g were anesthetized, and the sterilized occluders were implanted subcutaneously. The SD rats were euthanized at 1, 2, 4, 6, 8, and 12 weeks postsurgery. At each time point, three occluders and the adjacent tissues were collected for gross observation and histological analysis. After fixing in 10% neutral buffered formalin for 24 h, adjacent tissues were immersed in paraffin for 5 h. A tissue sectioner (RM2235, Leica, Germany) was used to cut the adjacent tissues longitudinally into 5 μm thick slices and the slices were mounted on glass slides. A hematoxylin-eosin staining kit (WLA051A, China) was used for light microscopic examination (DP73, OLYMPUS, Japan). Six parts of each slice were stained.

Preparation of the ASD Models: Six fresh isolated heart specimens were collected from healthy adult porcine models. The cardiac structure remained intact. The ends of superior, inferior vena cava, pulmonary vein, aorta and pulmonary artery remained for ≈15 mm. An ASD model was established by Brokenbrough needle puncture combined with balloon dilatation,^[61] and the puncture site was selected at 75° to the right anterior obliquity. A 14 Fr.*16 cm short catheter (Starway Medical Technology, Inc.) was used during the process, and the puncture needle was delivered by the catheter from the right atrium to the left atrium. An ASD with a diameter of ≈8 mm was established by balloon dilation three times.

Feasibility Tests of ASD Occlusion Devices In Vitro: After preparation of the ASD model, six 4-arm occluders were loaded into the catheter in turn and were pushed out of the catheter tip by a guide wire into the left atrium. The occluders were driven by injecting a hot physiological saline solution (67 °C) into the other side of the sheath. When the left disc of the occluder was deployed in the left atrial cavity, the catheter was withdrawn to ensure that the occluder clung to the atrial septal. Finally, the occluder was released, and the closure was completed.

Supporting Information

Supporting Information is available from the Wiley Online Library or from the author.

Acknowledgements

The authors gratefully acknowledge the financial supports provided by the National Natural Science Foundation of China (Grant Nos. 11632005 and 11672086). The authors also thank Dr. Xin Lan, Chao Li, and Xiaozhou Xin for their kind help.

Conflict of Interest

The authors declare no conflict of interest.

Keywords

4D printing, atrial septal defects, biodegradable occluder, remotely controllable, shape memory polymers

Received: August 11, 2019
Revised: September 20, 2019
Published online:

- [1] S. C. Mitchell, S. B. Korones, H. W. Berendes, *Circulation* **1971**, *43*, 323.
- [2] S. Jategaonkar, W. Scholtz, H. Schmidt, D. Fassbender, D. Horstkotte, *Clin. Res. Cardiol.* **2010**, *99*, 183.
- [3] F. Godart, A. Houejeh, M. Recher, C. Francart, A. Polge, M. Richardson, M. Cajot, A. Duhamel, *Arch. Cardiovasc. Dis.* **2015**, *108*, 57.
- [4] S. Liu, K. Peng, C. Hsiao, K. Liu, H. Chung, J. Chen, *Ann. Biomed. Eng.* **2011**, *39*, 2759.
- [5] Y. Y. Huang, Y. S. Wong, J. N. Chan, S. S. Venkatraman, *J. Mater. Sci.: Mater. Med.* **2015**, *26*, 93.
- [6] R. Hoehn, C. Hesse, H. Ince, M. Peuster, *Catheter. Cardiovasc. Interv.* **2010**, *75*, 72.
- [7] W. Lu, W. Ouyang, S. Wang, Y. Liu, F. Zhang, W. Wang, X. Pan, *J. Interv. Cardiol.* **2018**, *31*, 841.
- [8] Y. Zhu, X. Huang, J. Cao, J. Hu, Y. Bai, H. Jiang, Z. Li, Y. Chen, W. Wang, Y. Qin, X. Zhao, *J. Biomed. Biotechnol.* **2012**, *2012*, 1.
- [9] Y. Huang, Y. S. Wong, H. C. A. Ng, F. Y. C. Boey, S. Venkatraman, *Bioeng. Transl. Med.* **2017**, *2*, 156.
- [10] Y. Huang, J. F. Kong, S. S. Venkatraman, *Acta Biomater.* **2014**, *10*, 1088.
- [11] S. H. Jariwala, G. S. Lewis, Z. J. Bushman, J. H. Adair, H. J. Donahue, *3D Print. Addit. Manuf.* **2015**, *2*, 56.
- [12] M. Vukicevic, B. Mosadegh, J. K. Min, S. H. Little, *JACC* **2017**, *10*, 171.
- [13] D. C. Ackland, D. Robinson, M. Redhead, P. V. S. Lee, A. Moskaljuk, G. Dimitroulis, *J. Mech. Behav. Biomed. Mater.* **2017**, *69*, 404.
- [14] A. Goyanes, U. Det-Amornrat, J. Wang, A. W. Basit, S. Gaisford, *J. Controlled Release* **2016**, *234*, 41.
- [15] S. Bose, S. Vahabzadeh, A. Bandyopadhyay, *Mater. Today* **2013**, *16*, 496.
- [16] A. Kumar, S. Mandal, S. Barui, R. Vasireddi, U. Gbureck, M. Gelinsky, B. Basu, *Mater. Sci. Eng., R* **2016**, *103*, 1.
- [17] S. Miao, N. Castro, M. Nowicki, L. Xia, H. Cui, X. Zhou, W. Zhu, S. Lee, K. Sarkar, G. Vozzi, Y. Tabata, J. Fisher, L. G. Zhang, *Mater. Today* **2017**, *20*, 577.
- [18] J. Leng, X. Lan, Y. Liu, S. Du, *Prog. Mater. Sci.* **2011**, *56*, 1077.
- [19] C. Wischke, A. T. Neffe, S. Steuer, A. Lendlein, *J. Controlled Release* **2009**, *138*, 243.
- [20] F. S. Senatov, K. V. Niaza, M. Y. Zadorozhnyy, A. V. Maksimkin, S. D. Kaloshkin, Y. Z. Estrin, *J. Mech. Behav. Biomed. Mater.* **2016**, *57*, 139.
- [21] M. Zarek, N. Mansour, S. Shapira, D. Cohn, *Macromol. Rapid Commun.* **2017**, *38*, 1600628.
- [22] Q. Zhao, J. Wang, H. Cui, H. Chen, Y. Wang, X. Du, *Adv. Funct. Mater.* **2018**, *28*, 1801027.
- [23] A. Lendlein, M. Behl, B. Hiebl, C. Wischke, *Expert Rev. Med. Devices* **2010**, *7*, 357.
- [24] A. Metcalfe, A. Desfaits, I. Salazkin, L. H. Yahia, W. M. Sokolowski, J. Raymond, *Biomaterials* **2003**, *24*, 491.
- [25] P. Singhal, W. Small, E. Cosgriff-Hernandez, D. J. Maitland, T. S. Wilson, *Acta Biomater.* **2014**, *10*, 67.
- [26] A. J. Boyle, T. L. Landsman, M. A. Wierzbicki, L. D. Nash, W. Hwang, M. W. Miller, E. Tuzun, S. M. Hasan, D. J. Maitland, *J. Biomed. Mater. Res., Part B* **2016**, *104*, 1407.
- [27] C. M. Yakacki, K. Gall, in *Shape-Memory Polymers* (Ed: A. Lendlein), Springer, Berlin **2010**, p. 147.
- [28] J. Chen, J. Hu, A. K. L. Leung, C. Chen, J. Zhang, Y. Zhang, Y. Zhu, J. Han, *ACS Appl. Mater. Interfaces* **2018**, *10*, 32935.
- [29] W. Zhao, L. Liu, F. Zhang, J. Leng, Y. Liu, *Mater. Sci. Eng., C* **2019**, *97*, 864.
- [30] C. M. Yakacki, R. Shandas, C. Lanning, B. Rech, A. Eckstein, K. Gall, *Biomaterials* **2007**, *28*, 2255.
- [31] R. Xie, J. Hu, O. Hoffmann, Y. Zhang, F. Ng, T. Qin, X. Guo, *Biochim. Biophys. Acta, Gen. Subj.* **2018**, *1862*, 936.
- [32] S. Tibbits, presented at *TED Conference*, February **2013**.
- [33] Q. Ge, A. H. Sakhaei, H. Lee, C. K. Dunn, N. X. Fang, M. L. Dunn, *Sci. Rep.* **2016**, *6*, 31110.
- [34] M. Lin, N. Firoozi, C. Tsai, M. B. Wallace, Y. Kang, *Acta Biomater.* **2019**, *83*, 119.
- [35] J. Huang, J. Ren, G. Wang, Z. Li, X. Wu, H. Ren, S. Liu, *World J. Gastroenterol.* **2017**, *23*, 7489.
- [36] T. Serra, M. Ortiz-Hernandez, E. Engel, J. A. Planell, M. Navarro, *Mater. Sci. Eng., C* **2014**, *38*, 55.
- [37] M. O. Wang, C. E. Vorwald, M. L. Dreher, E. J. Mott, M. Cheng, A. Cinar, H. Mehdizadeh, S. Somo, D. Dean, E. M. Brey, J. P. Fisher, *Adv. Mater.* **2015**, *27*, 138.
- [38] C. Deng, Q. Yao, C. Feng, J. Li, L. Wang, G. Cheng, M. Shi, L. Chen, J. Chang, C. Wu, *Adv. Funct. Mater.* **2017**, *27*, 1703117.
- [39] B. Yang, J. Yin, Y. Chen, S. Pan, H. Yao, Y. Gao, J. Shi, *Adv. Mater.* **2018**, *30*, 1705611.
- [40] J. L. Corchero, A. Villaverde, *Trends Biotechnol.* **2009**, *27*, 468.
- [41] N. S. Satarkar, J. Z. Hilt, *J. Controlled Release* **2008**, *130*, 246.
- [42] Y. Li, G. Huang, X. Zhang, B. Li, Y. Chen, T. Lu, T. J. Lu, F. Xu, *Adv. Funct. Mater.* **2013**, *23*, 660.
- [43] A. P. A. J. Q., *J. Phys. D: Appl. Phys.* **2003**, *36*, R167.
- [44] C. A. Cezar, S. M. Kennedy, M. Mehta, J. C. Weaver, L. Gu, H. Vandenburg, D. J. Mooney, *Adv. Healthcare Mater.* **2014**, *3*, 1869.
- [45] C. Fang, F. M. Kievit, O. Veiseh, Z. R. Stephen, T. Wang, D. Lee, R. G. Ellenbogen, M. Zhang, *J. Controlled Release* **2012**, *162*, 233.
- [46] M. P. Prabhakaran, J. Venugopal, S. Ramakrishna, *Acta Biomater.* **2009**, *5*, 2884.
- [47] L. Ghasemi-Mobarakeh, M. P. Prabhakaran, M. Morshed, M. Nasr-Esfahani, S. Ramakrishna, *Biomaterials* **2008**, *29*, 4532.
- [48] Q. Yao, J. G. L. Cosme, T. Xu, J. M. Miszuk, P. H. S. Picciani, H. Fong, H. Sun, *Biomaterials* **2017**, *115*, 115.
- [49] L. Jiang, J. Zhang, M. P. Wolcott, *Polymer* **2007**, *48*, 7632.
- [50] Y. Huang, Y. S. Wong, J. Wu, J. F. Kong, J. N. Chan, L. Khanolkar, D. P. Rao, F. Y. C. Boey, S. S. Venkatraman, *J. Mech. Behav. Biomed. Mater.* **2014**, *36*, 143.
- [51] Z. H. Tu, V. P. W. Shim, C. T. Lim, *Int. J. Solids Struct.* **2001**, *38*, 9267.
- [52] R. Liu, P. Zhang, Q. Zhang, Q. Zhou, H. Dai, *J. Mech. Behav. Biomed. Mater.* **2018**, *82*, 9.
- [53] E. Fournier, C. Passirani, C. N. Montero-Menei, J. P. Benoit, *Biomaterials* **2003**, *24*, 3311.
- [54] Y. Ramot, M. Haim-Zada, A. J. Domb, A. Nyska, *Adv. Drug Delivery Rev.* **2016**, *107*, 153.
- [55] X. Huang, Y. Zhu, J. Cao, J. Hu, Y. Bai, H. Jiang, Z. Li, Y. Chen, W. Wang, Y. Qin, *Catheter. Cardiovasc. Interv.* **2013**, *81*, 324.
- [56] B. Gupta, N. Revagade, J. Hilborn, V. Teknisk-naturvetenskapliga, Polymerkemi, U. Uppsala, F. M. Institutionen, S. Kemiska, *Prog. Polym. Sci.* **2007**, *32*, 455.
- [57] C. Jux, P. Wohlsein, M. Bruegmann, M. Zutz, B. Franzbach, H. Bertram, *J. Interv. Cardiol.* **2003**, *16*, 149.
- [58] Y. S. Wong, A. V. Salvekar, K. Da Zhuang, H. Liu, W. R. Birch, K. H. Tay, W. M. Huang, S. S. Venkatraman, *Biomaterials* **2016**, *102*, 98.
- [59] J. Wang, Q. Zhao, H. Cui, Y. Wang, H. Chen, X. Du, *J. Mater. Chem. A* **2018**, *6*, 24748.
- [60] J. Wang, Q. Zhao, Y. Wang, Q. Zeng, T. Wu, X. Du, *Adv. Mater. Technol.-Us* **2019**, <https://doi.org/10.1002/admt.201900566>.
- [61] T. D. King, N. L. Milk, *Surgery* **1974**, *75*, 383.